Multiscale QM/MM Molecular Dynamics Simulations of the Trimeric Major Light-Harvesting Complex II

Sayan Maity,[†] Vangelis Daskalakis,[‡] Marcus Elstner,[¶,§] and Ulrich Kleinekathöfer[*,†]

[†]*Department of Physics and Earth Sciences, Jacobs University Bremen, Campus Ring 1, 28759 Bremen, Germany*

[‡]*Department of Chemical Engineering, Cyprus University of Technology, 30 Archbishop Kyprianou Str. 3603, Limassol, Cyprus*

[¶]*Institute of Physical Chemistry, Karlsruhe Institute of Technology (KIT), Kaiserstrasse 12, 76131 Karlsruhe, Germany*

[§]*Institute of Biological Interfaces (IBG2), Karlsruhe Institute of Technology (KIT), Kaiserstrasse 12, 76131 Karlsruhe, Germany*

E-mail: u.kleinekathoefer@jacobs-university.de

Abstract

Photosynthetic processes are driven by sunlight. Too little of it and the photosynthetic machinery cannot produce the reductive power to drive the anabolic pathways. Too much sunlight and the machinery can get damaged. In higher plants, the major Light Harvesting Complex (LHCII) efficiently absorbs the light energy, but can also dissipate it when in excess (quenching). In order to study the dynamics related to the quenching process but also the exciton dynamics in general, one needs

to accurately determine the so-called spectral density which describes the coupling between the relevant pigment modes and the environmental degrees of freedom. To this end, Born–Oppenheimer molecular dynamics simulations in a quantum mechanics/molecular mechanics (QM/MM) fashion utilizing the density functional based tight binding (DFTB) method have been performed for the ground state dynamics. Subsequently, the time-dependent extension of the long-range-corrected DFTB scheme has been employed for the excited state calculations of the individual chlorophyll-a molecules in the LHCII complex. The analysis of this data resulted in spectral densities showing an astonishing agreement with the experimental counterpart in this rather large system. This consistency with an experimental observable also supports the accuracy, robustness, and reliability of the present multi-scale scheme. In addition, the resulting spectral densities and site energies were used to determine the exciton transfer rate within a special pigment pair consisting of a chlorophyll-a and a carotenoid molecule which is assumed to play a role in the balance between the light harvesting and quenching modes.

Introduction

Photosynthesis is one of the key processes for life on earth. Phototrophic organisms capture the sunlight and convert it into chemical energy. Subsequently, this energy is also accessible to heterotrophic organisms such as animals, fungi and many bacteria. In green plants and algae, thylakoid membranes host supramolecular pigment-protein aggregates including the photosystem I (PSI) and II (PSII) complexes together with antenna systems. These antennas in the thylakoid membrane are responsible for the first steps of photosynthesis enabling light harvesting and excitation energy transfer (EET) processes among the pigments at an ultrafast timescale. In plants, chlorophyll-a (Chl-a), b (Chl-b) and carotenoid molecules are the main players primary contributing to light harvesting. Well-orchestrated networks of pigments have the ultimate goal of directing energy in the form of excitons from the antennas to the PSI/PSII reaction centers (RCs) where charge separation takes place[1]. During these

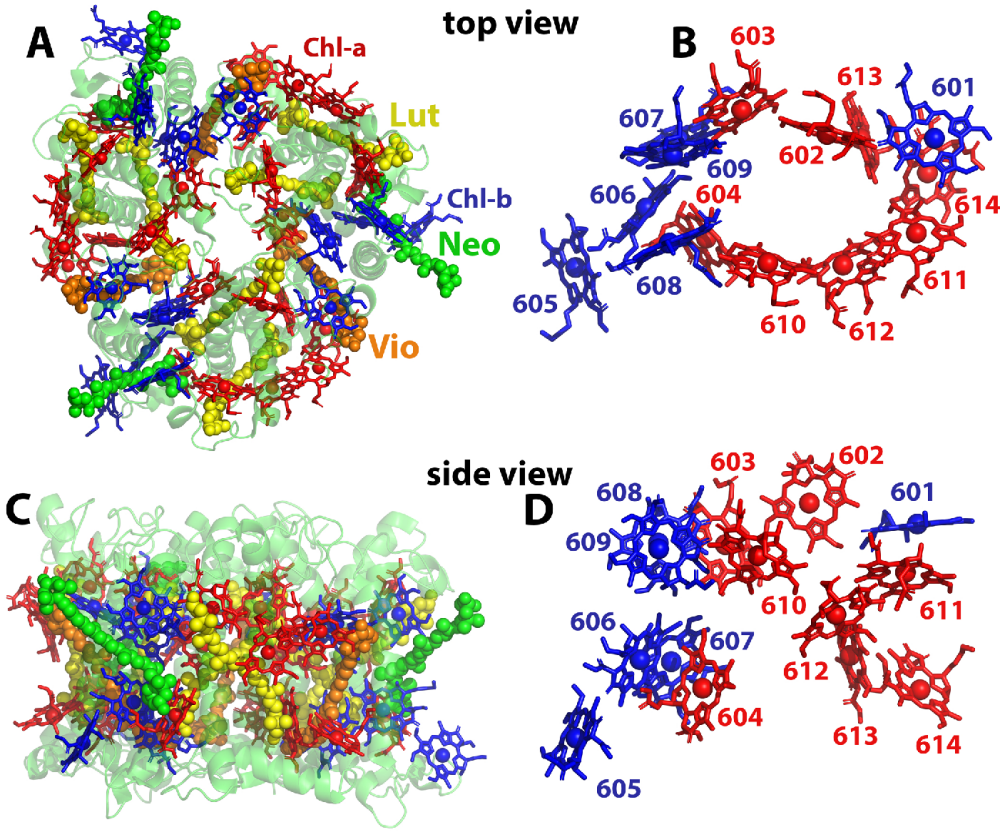

Figure 1: Structure of the major LHCII trimer. A) top view of the LHCII trimer in green cartoon representation. The protein is shown transparently for visualization purposes while the Chl-a molecules are shown in red, the Chl-b molecules in blue and the three different types of carotenoids in yellow, green, and orange. B) The chlorophylls of one monomeric unit are shown separately. C, D) Side views corresponding to panels A and B.

energy transfer processes, a pH gradient is built up across the thylakoid membrane, which is also utilized to fine tune the photosynthetic load under fluctuating light intensities in order to reduce potential photochemical damage. Under conditions of excess light, the fastest regulation is triggered by this enhanced trans-thylakoid pH gradient. The latter is part of a process termed non-photochemical quenching (NPQ) of higher plants[2–5]. The self-regulation of light harvesting within the thylakoid membranes is very important for the organism since the PSII complex is highly susceptible to photodamage under excess light conditions[6,7]. This self-regulation occurs on the molecular level by aggregation and allosteric regulation of the major light-harvesting complex (LHCII) attached to the PSII system[4,8,9]. The antenna complexes of PSII mainly consist of LHCII trimers (see Fig. 1)

with each monomer binding fourteen chlorophyll molecules (eight Chl-a, six Chl-b) and four carotenoid molecules namely two luteins (Lut), one neoxanthin (Neo), and one violaxanthin (Vio)[10]. The Chl-b molecules are present in the periphery of the antenna complexes. Their auxiliary role is to harvest blue-shifted sunlight and transfer it to the Chl-a pool[11,12]. The sunlight excites the Chl-a molecules mainly into their lowest singlet excited state (termed S1 or Q_y), prior to being transferred/spread among the pigments, mainly of the same kind, with a quantum efficiency close to one[13]. In this study, the focus is on the light harvesting mode of the LHCII trimer, in which the Chl-a molecules play a key role and the carotenoids are mainly responsible for its regulation[4]. Experiments carried out by Novoderezhkin et al.[14] identified fast relaxation rates between the strongly coupled 606-607 and 608-609 Chl-b dimers, as well as the Chl-a 602-603, 613-614 pairs and the 610-611-612 triples. Further investigations by Schlau-Cohen et al.[15] and Zucchelli et al.[16] have indicated Chl-a 612 as one of the most red shifted Chl molecules in the LHCII that acts as the terminal emitter towards the RC. However, Müh et al.[17] suggested that within LHCII, the three Chl-a molecules 610-611-612 constitute a potential energy sink and that the Chl-a 610 pigment has the lowest site energy at cryogenic temperatures. Finally, from this emitter domain, the excitonic energy is mainly directed to the minor antenna, i.e., the CP29 complex, the core of the PSII, and to the RCs[18]. Furthermore, Müh et al.[17] found that the pigments Chl-a 602, 603, 604, and 613 may contribute to the red edge of the absorption spectrum of the LHCII complex and that especially Chl-a 604 can act as a bottleneck for the energy transfer with its site energy being strongly influenced by the protein environment. These partially conflicting findings suggest that in order to understand the energy transfer process in the LHCII complex properly, the Chl-a pool needs to be analyzed in more detail and an accurate description of the ground and excited state electronic structures of the Chl-a molecules becomes a necessity.

In experiment, often two-dimensional electronic spectroscopy is used to study LH complexes[19]. To calculate the excitation energy transfer dynamics among the pigments, one needs to use the concept of open quantum systems either fully quantum mechanically or

within a mixed quantum-classical description[20]. Two different types of approaches are often employed, i.e., either a density matrix or an ensemble-averaged wave-packet formalism[21–23]. For the former, the spectral density is a key ingredient and combined with the time-averaged Hamiltonian this quantity is employed to propagate the density matrix of the system. For the latter case, a time-dependent Hamiltonian is constructed consisting of the excitation energies and excitonic coupling values based on which an ensemble-averaged wave packet dynamics can be performed. The latter approach usually involves more approximations leading to problems in reaching the proper thermal equilibrium in case of Ehrenfest dynamics or by including dephasing in case of surface hopping. A wealth of different density matrix approaches exists with the hierarchy equation of motion (HEOM) approach being one of the more popular ones in the field of exciton transfer in LH complexes[21,24–26]. This scheme has the advantage that it can be converged with respect to the system-bath coupling strength. It assumes that the spectral density can be written as a form of Lorentzian functions while numerically it can be quite expensive[24,27]. One way to obtain some of the necessary ingredients for these quantum dynamics schemes are classical molecular dynamics (MD) simulations followed by excitation energy calculations along the trajectories[22,28–32]. In such a scheme, often the ZINDO/S-CIS (Zerner's Intermediate Neglect of Differential Orbital method with spectroscopic parameters together with the configuration interaction using single excitation) approach or variants of the time-dependent density functional theory (TDDFT) were applied to obtain the excitation energies along a trajectory in a quantum mechanics/molecular mechanics (QM/MM) fashion. In recent benchmark studies it became clear that the description of the excitation energy fluctuations along trajectories are more accurate using (long range-corrected) TDDFT theories than the semi-empirical ZINDO/S-CIS approach[22,33]. One should keep in mind that the TDDFT approaches suffer from an overestimation of the absolute excitation energies but for the excitation energy transfer dynamics only relative energies are of importance.

Apart from the exciton dynamics on a femtosecond to picosecond time scale, also the

excitonic lifetimes on the nanosecond time scale are of interest. This need is especially high for LH complexes of plants since within that time regime the pH value on the lumenal side of the thylakoid membrane can be shifted to trigger the photoprotection in the antenna systems. In order to calculate the lifetimes of the excited states, the Förster rate constant of the excitation transfer can be determined based on Fermi's golden rule where the site energy, spectral density and excitonic coupling values are necessary input parameters[9,34]. Hence, a similar multi-scale strategy based on an MD simulation followed by an excited state analysis within a mixed approach can be utilized to describe the excitonic lifetimes.

Although mixed quantum-classical approaches on top of a classical MD trajectory can provide a reasonable description of the system, these scheme encounter the so-called "geometry mismatch" problem arising due to the inconsistency of the force-field based coordinates and the electronic structure calculations[30,35,36]. This mismatch in geometry generates artifacts in the spectral density and thus can subsequently affect the exciton dynamics as well as the transfer rates to some extent. Another manifestation of the same problem is that the representation of the internal vibrational modes of the pigments in classical MD schemes is limited by the accuracy of the employed force fields. To overcome these problems, Rhee and co-workers have proposed to propagate the system on a pre-determined quantum mechanical potential energy surface (PES) for the ground state and calculated the excitation energies based on the respective pre-determined interpolated excited state PES[37]. Furthermore, Coker and co-workers suggested an alternative formalism to accurately describe the intra-molecular part of spectral densities[38]. Although, both approaches provide an impressive agreement between the theoretical and experimental spectral densities taking into account the size of the studied system, they suffer from high numerical costs required to construct the PES[39] or to determine the normal mode analysis while calculating the intra-molecular contribution at a high level of accuracy[40]. A reliable ground state QM/MM MD dynamics followed by excitation calculations using a high level QM method would be an ideal choice to accurately describe the dynamics of the energy gap for pigment molecules. However, because

of the size of the pigments in LH systems, it is numerically challenging to perform state of the art QM/MM MD simulations based on DFT[25] or even semi-empirical methods[41]. In this direction, our recent protocol based on the density functional tight-binding (DFTB) level of theory[42] is a numerically affordable alternative to perform an accurate ground state dynamics followed by excited state calculations for the relatively large pigment molecules[33,43]. Based on this strategy, in the present contribution we report on a DFTB-QM/MM MD ground state dynamics for the Chl-a molecules in connection with a classical description of the environment based on the OPLS force field. Subsequently, the time-dependent long-range-corrected extension of DFTB (TD-LC-DFTB)[44] has been applied again in a QM/MM setting along those QM/MM MD trajectories to determine the energy gap fluctuation of each pigment. We found that the average spectral densities calculated using this scheme show a remarkable agreement compared with the results of fluorescence line narrowing (FLN) experiments of the LHCII complex. The accurate description of the major peaks clearly demonstrates the power of the DFTB-based QM/MM MD for the biologically relevant LH complexes. Finally, the spectral densities and the average site energies averaged on a nanosecond timescale have been utilized to determine the excitation transfer rate within the Chl-a 612/Lut-1 pair based on our previously reported excitonic couplings for the low and neutral lumenal pH states of the LHCII complex[9].

Computational Method

As starting structure, the solvated trimeric LHCII complex (pdb code 1RWT, chains C, E, H) was modeled with roughly 221k atoms and equilibrated under low (pH $\sim$ 5.5) and neutral lumenal pH (pH $\sim$ 7) as described in Ref. 9. The carboxylic groups belonging to side chains of lumen exposed residues in each monomeric unit (GLU E-83, 94, 107, 207 and ASP D-111, 211, 215) have been treated as protonated (-COOH) or deprotonated (-COO^-) to mimic the low and neutral lumenal pH state of the system, respectively. These titratable polypeptide residues have been predicted in experiment[45–47], modeled using the PDB2PQR server with

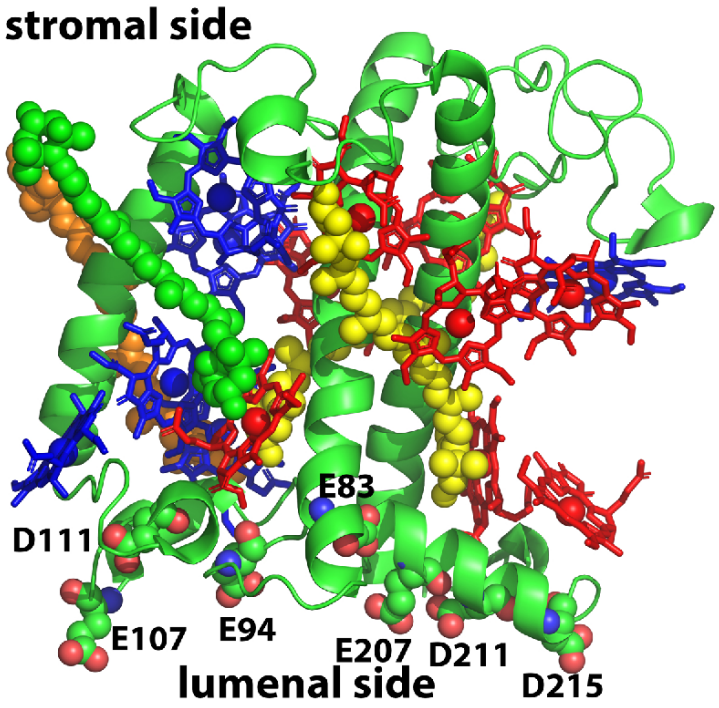

Figure 2: Lumen exposed residues in one monomer unit of the LHCII complex which have been protonated or deprotonated to mimic the two different lumenal pH states.

the PROPKA approach[9,48] and are highlighted in Fig. 2 in van der Waals representation. For each pH state, three simulations were performed to obtain a reasonable sampling of the available phase space for converged spectral densities based on the QM/MM ground state dynamics. The initial structures for these sets have been extracted in an equally spaced manner from 1.5 μs long classical MD simulations for both pH states as reported in Ref. 9. As the crystal structure conformation of the LHCII complex refers to the quenched state[2,49,50], the system built at low lumenal pH is assumed to be trapped in conformations close to the crystal geometry during the unbiased simulations. In case of the QM/MM ground state dynamics as well as the excitation energy calculations, the phytyl tail of the Chl-a molecule under investigation was truncated at the C1-C2 bond and capped by an H atom. Subsequently, the truncated Chl-a molecule has been considered as the QM region in the QM/MM calculations. The third-order version of DFTB with the 3OB-f parameter set (DFTB3/3OB-f) has been employed to perform the ground state dynamics combined with the OPLS force field for the classical description of the environment. The 3OB-f is a

variant of the standard 3OB set with an optimized description of the vibrational frequencies which especially improves the C=C, C=O and C=N stretching modes within the DFTB framework[51,52]. This enhancement has already shown to yield very reasonable results for the spectral densities in the bacterial Fenna-Matthews-Olson (FMO) complex[43]. For each pigment, a 60 ps NPT simulation with a 0.5 fs time step was carried out at 300 K using the GROMACS/DFTB+ interface[33,53,54]. Snapshots were stored for the last 40 ps of the dynamics with a stride of 1 fs. This scheme produces 40,000 frames per pigment which then served as input coordinates for the excitation energy calculations in the subsequent step. Thus, for both low and neutral pH, a total of 2×24×40,000 frames were generated for the 24 Chl-a pigments in the LHCII trimer since the current DFTB/MM implementation can only handle one QM region at a time. The same number of frames were also produced for the other two sets of initial coordinates out of the 1.5 μs trajectories. Moreover, we have extended the first set of simulations up to 1.1 ns with a 1 fs time step. For the last 1 ns the snapshots were stored every 1 ps. This scheme produced another 1,000 frames for each of the 2 × 24 QM/MM MD simulations which were then utilized to determine the average excitation energies on a nanosecond timescale.

The excitation energies along the ground state trajectories were calculated with the help of the DFTB+ code in which the time-dependent extension of long-range corrected DFTB method is implemented with the OB2 parameter set (TD-LC-DFTB/OB2)[44,54,55]. Furthermore, during the excitation energy calculations, the QM region has been shifted towards the center of the simulation box with the MM region being moved accordingly which is possible due to the periodic boundary condition. This kind of treatment is necessary to avoid artificial boundary effects in the non-periodic QM/MM excited state calculations[56,57]. The computational costs for the ground state QM/MM MD and the excited QM/MM calculations were similar to those of our previous study for a bacterial system[43] while numerically being cheaper than DFT-based approaches with similar accuracy[33]. After performing the TD-LC-DFTB calculations, the energies of the first excited state have been extracted along

the QM/MM MD trajectories. This first excited state, i.e., the Q_y state, plays a major role in the light absorption as well as in the energy transfer among the Chl molecules. In a last step, the autocorrelation functions of the excitation energies are determined followed by a calculation of the spectral densities as described in the following section.

Results and Discussion

Site Energy Calculations

To be able to perform the exciton dynamics within LH systems, usually a tight-binding Hamiltonian H_S of the system is constructed[20,58]. Generally, the Hamiltonian has the following generic form

$$H_S = \sum_m E_m \left|m\right\rangle \left\langle m\right| + \sum_{n \neq m} V_{mn} \left|n\right\rangle \left\langle m\right| \tag{1}$$

where E_m denotes the excitation energy gap of pigment m which is also called the site energy and V_{mn} is the excitonic coupling between pigment molecules m and n. Depending on the theory used for the exciton dynamics, the Hamiltonian is either used directly in its time-dependent variant or averaged over time to get a time-averaged Hamiltonian. Moreover, diagonalizing the Hamiltonian yields the excitonic energies and states in a time-dependent or time-averaged fashion. In this study, the site energy for each Chl-a molecule in the LHCII trimer is determined at the TD-LC-DFTB level along the respective QM/MM MD trajectory. The average site energies for the first set of the 40 ps and the 1 ns QM/MM MD trajectories are shown in Fig. 3 for the low and neutral lumenal pH states. No significant differences in the site energies of the individual pigments can be observed for the two different pH states which is not completely surprising due to the quite similar electrostatic environment at the two different pH values. Moreover, the average excitation energies of the Chl-a molecules based on TD-LC-DFTB are in the same range as those from TDDFT calculations determined using the CAM-B3LYP functional[59]. This finding is consistent with our recent benchmark study where we have shown that the TD-LC-DFTB approach is an accurate alternative for

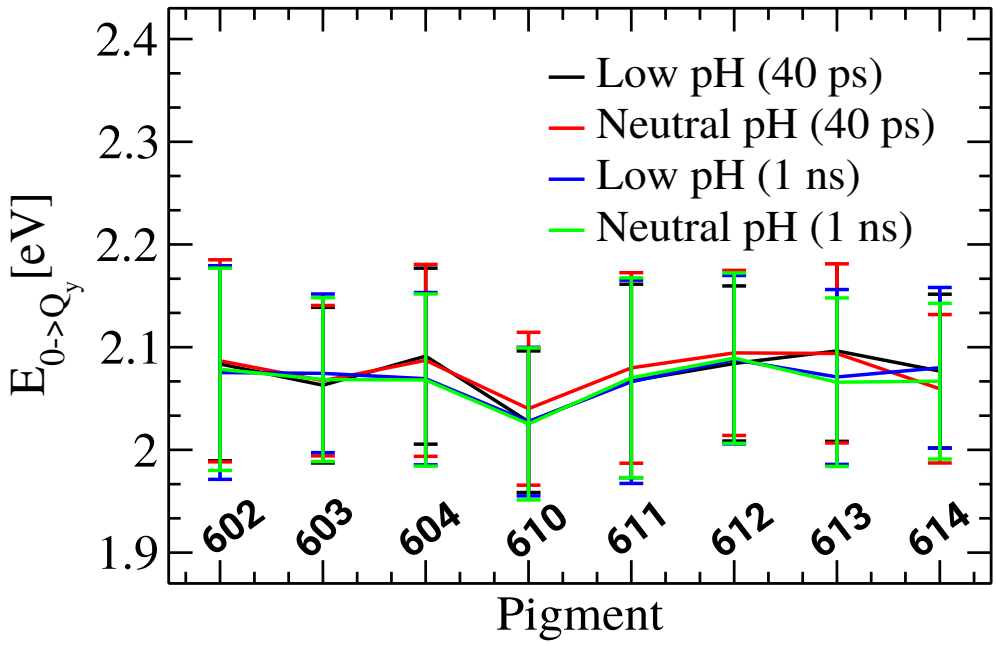

Figure 3: Average site energies and associated standard deviations for the Chl-a pigments in the LHCII complex based on QM/MM MD trajectories and subsequent TD-LC-DFTB excited state calculations. The results for the first set of the 40 ps and the 1 ns QM/MM MD trajectories at both pH values are depicted. For each pigment the site energy is averaged over the equivalent molecules in the three monomer units.

the calculation of excitation energies in natural LH systems. Long-range corrected (LC) and hybrid functionals (CAM-B3LYP, ωB97X, LC-BLYP, B3LYP etc.) within TDDFT theory can obtain reasonable results for the excited state calculations necessary in the present study. However, they are numerically quite expensive when performed along trajectories[33]. In other investigations, the semi-empirical ZINDO/S-CIS method has been employed along classical MD trajectories for the LHCII complex leading to site energy values close to the experimental ones[60]. Although, the ZINDO/S-CIS approach is numerically very efficient and results in average site energies of Chl and BChl molecules that are rather accurate due to its parametrization for this molecule class, the fluctuations and the influence of environmental charges are less well represented[33,43]. This inadequacy of the ZINDO/S-CIS scheme is likely due to its parametrization for equilibrium conformations but not out-of-equilibrium ones[61,62].

The corresponding site energy distributions of the eight pigments are of Gaussian shape as shown in Figs. S1 and S2. The shapes of the distributions look quite similar for the individual

monomers though not identical which shows that the sampling of the individual monomers is not yet perfect. Looking again at the average site energies in Fig. 3 and comparing the results of averaging over the 40 ps and the 1 ns dynamics, a small but clearly visible difference can be observed for some Chl-a molecules. The 1 ns QM/MM MD simulation is assumed to be sufficiently long for a proper sampling of the relevant conformations and gives some insight into the energy ladder of the LHCII complex. Despite the small differences, for all trajectories the pigment Chl-a 610 has the lowest average site energy in the Chl-a pool while one has to clearly state that the differences in the site energies are smaller than the respective standard deviations. Moreover, one needs to take into account the good but limited accuracy of DFTB but also other electronic structure theories, a fact which should not be forgotten when interpreting the small energy differences found in the present study. At any rate, the fact that the differences between the average energies are smaller than the standard deviations clearly shows that there is only a very weak energy funnel which drives the excitation energy in a certain direction. The present finding that Chl-a 610 has the lowest average site energy seems to disagree with the experimental observation that Chl-a 612 acts as terminal emitter of the LHCII complex[15]. At the same time, Müh et al.[17] have shown in their calculations that Chl-a 610 can achieve the lowest site energy at low temperatures but that the triplet Chl-a 610-611-612 should be considered as the terminal emitter of LHCII with some small variation at different physiological conditions. Structurally, Chl-a 610 is a special pigment coordinated to a native (structurally resolved) thylakoid lipid and not to a protein residue. Therefore, one can expect that its site energy is able to fluctuate substantially during the dynamics.

Spectral Density

In the context of theory of open quantum systems, the bath-induced spectral density is one of the key features for studying the exciton dynamics in LH complexes[20]. The spectral density describes the frequency-dependent coupling of selected modes of the pigment with

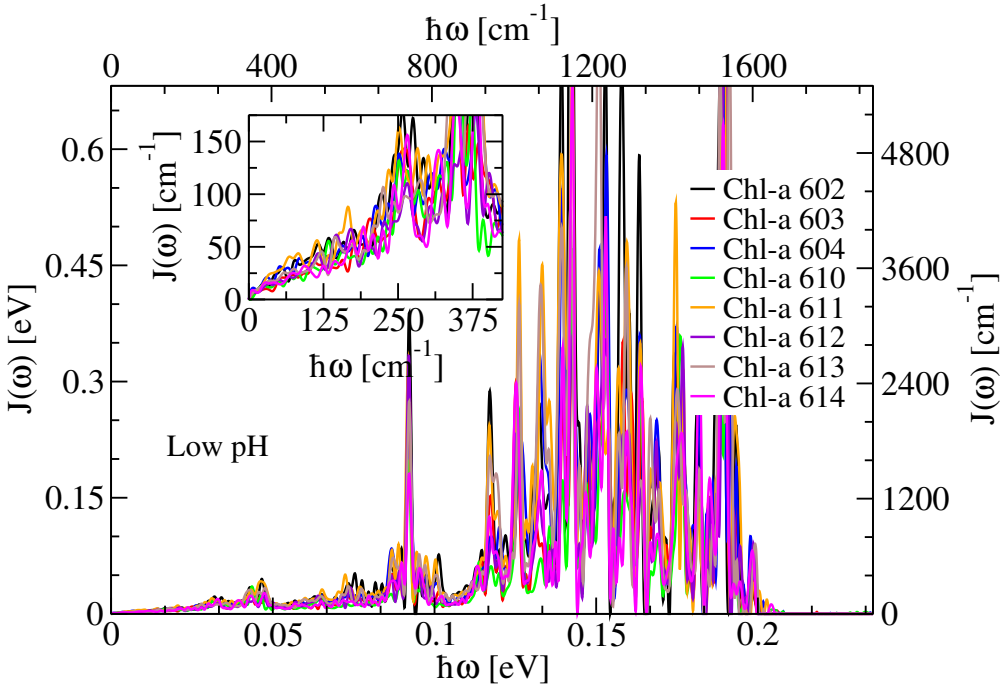

Figure 4: Spectral densities for the individual Chl-a pigments in the LHCII trimer in the low lumenal pH state based on first set of 40 ps QM/MM MD trajectory. The inset shows the low-frequency region. The spectral densities have been averaged over the equivalent chromophores in the three monomers.

environmental modes which also include modes of the system which do not belong to the primary system. There are various methods to obtain this quantity using different theoretical or experimental techniques. In this study we have employed a well-established technique which has been applied earlier to bacterial and algae LH complexes. In this formalism, a cosine transformation of the site-energy autocorrelation function decorated with a thermal factor is performed to determine the spectral density of each pigment molecule[22,36,43,63–65]. To this end, the spectral density of pigment m can be written as

$$J_m(\omega) = \frac{\beta\omega}{\pi} \int_0^\infty dt C_m(t) \cos(\omega t) \tag{2}$$

where $\beta = 1/k_B T$ denotes the inverse temperature. The site-energy autocorrelation function $C_m(t)$ can be determined from a time series of the energy gaps as

$$C_m(t_l) = \frac{1}{N-l} \sum_{k=1}^{N-l} \Delta E_m(t_l + t_k) \Delta E_m(t_k) \ . \tag{3}$$

In this expression E_m denotes the site energy, i.e., the energy difference between the Q_y and the ground state while $\Delta E_m = E_m - \langle E_m \rangle$ refers to the difference from its average. Moreover, we have employed the same windowing technique as well as zero padding as described in our recent study to compute the final autocorrelation functions and from them the corresponding spectral densities[43]. Here, the autocorrelation functions and the associated spectral densities have been extracted for a total of 24 Chl-a molecules for the LHCII trimer complex based on TD-LC-DFTB calculations along QM/MM MD trajectories (see Fig. S2). The spectral densities averaged over the equivalent pigments in the three monomers based on first set of 40 ps QM/MM MD trajectory are shown in Fig. 4 for the low lumenal pH state. The spectral densities computed at neutral lumenal pH have similar shapes like the ones at low lumenal pH (see Fig. S3 for a comparison).

As can be seen in Fig. 4, the major peaks of the spectral densities are in the range between 1030 and 1550 cm^{-1} which mainly represent collective intra-molecular vibrational modes which include C=C, C=O and C=N bond stretching[43]. The fastest oscillation periods in the corresponding autocorrelation function are in the range of about 22 to 32 fs as shown in the Fig. S2. In spite of having major peaks in the same frequency range, the amplitudes of these spectral density peaks differ substantially among the various Chl-a molecules. Since sampling issues were observed already in the spectral density calculations based on QM/MM MD trajectories for the FMO complex[43], three sets of QM/MM MD simulations were performed from where the autocorrelation functions and the associated spectral densities were determined. The comparison of the spectral densities based on these three sets of QM/MM MD trajectories is given in the Fig. S2 for both pH values. From this figure,

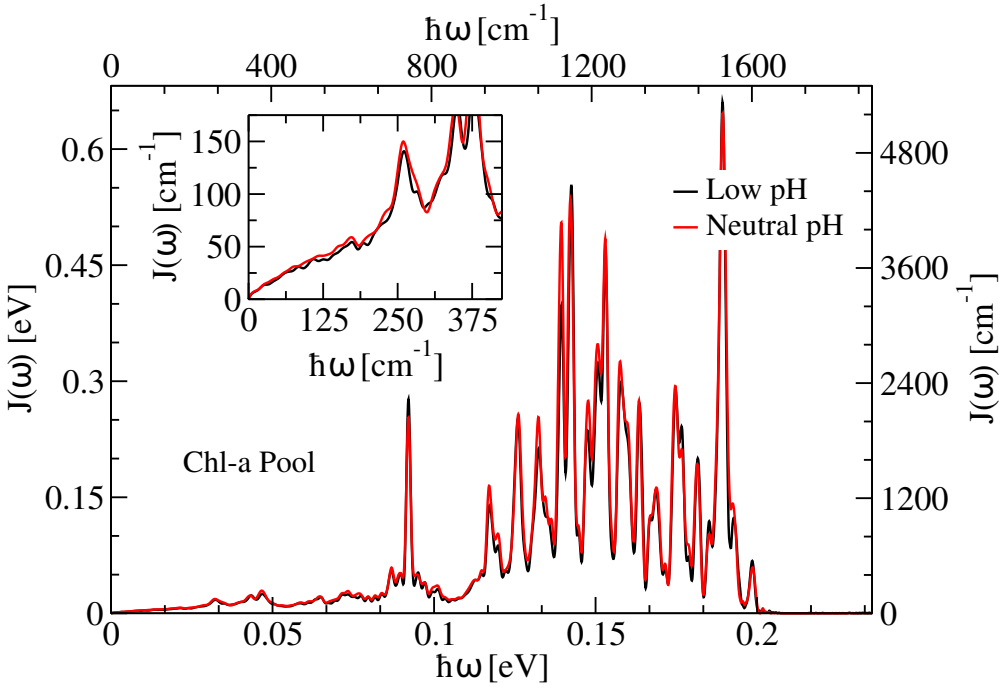

Figure 5: Spectral densities averaged over all 24 Chl-a molecules in the LHCII trimer at low and neutral lumenal pH states based on three sets of QM/MM MD trajectories. The inset shows the low-frequency region.

one can see that the intensities and positions of some major peaks are different in the three sets of QM/MM MD trajectories. Although, the calculated spectral densities for individual Chl-a have been averaged over the three monomers, a moderate sampling issue still can be observed. The average spectral density over all pigments in the Chl-a pool is assumed to be converged when comparing the results for the three sets of QM/MM dynamics. This finding suggests that the sampling issue can be eliminated by averaging over longer time series and/or more simulations. One has to keep in mind that at the beginning of a dynamical simulation usually not all modes are excited to the same extent and thus these modes appear with different intensity in the cosine transform until the sampling is good enough. Here, we would like to point out that this issue was not observed, at least not to the present degree, for the spectral densities based on classical MD trajectories. In the latter case, the amount of sampling needed for a proper reproducibility was smaller which might indicate a faster energy redistribution among the modes in classical MD simulations[43,56]. In the final steps,

we have averaged the spectral densities from the three sets of QM/MM MD trajectories over all pigments within the Chl-a pool. This procedure has been performed for both pH values and the results are displayed in Fig. 5. Only small differences between the average spectral densities can be seen. This outcome is not very surprising since the residues in the local neighborhoods of the pigment molecules exert subtle changes between the different pH states shown in our previous work[9]. Anyhow, the environment would only influence the low-frequency part of the spectral densities while the medium to high-frequency portion of the spectral density is governed by internal modes. At the same time, the reproducibility of the spectral density from different initial coordinates for the two pH states is reassuring highlighting the robustness of the employed scheme for the determination of the spectral densities.

Considering the robustness of our results, it is of course interesting to see how accurate they are. To this end, we turn to the experimentally determined spectral density for the LHCII complex[66]. This spectral density $J^{exp}(\omega)$ was modeled using a combination of Drude and Lorentzian functions using the following expression[66,67]

$$J^{exp}(\omega) = \frac{2\hbar}{\pi}\lambda\gamma\frac{\omega}{(\omega^2+\gamma^2)} + \frac{2\hbar}{\pi}\sum_k s_k\omega_k^3\frac{\omega\gamma_k}{(\omega_k^2-\omega^2)^2+\omega^2\gamma_k^2} \ . \tag{4}$$

The first part of this expression has been designed to mainly describe the low frequency modes due to the electrostatic coupling to the environment. It has been modeled as an over-damped Brownian oscillator. The second part of the expression for $J^{exp}(\omega)$ is given by a sum over Lorentzian functions based on a modeling of the high-frequency modes as under-damped Brownian oscillators[67]. The electron-phonon and electron-vibrational coupling parameters , i.e., λ, γ , s_k, and ω_k, have been determined based on fluorescence line narrowing (FLN) measurements and are listed in Tables 1 and 2 of Ref. 66. The same frequencies of vibrational modes have also been reported in Ref. 67 for the complete PSII super-complex (not only LHCII) with slightly different peak intensities and/or widths. In the expression for the

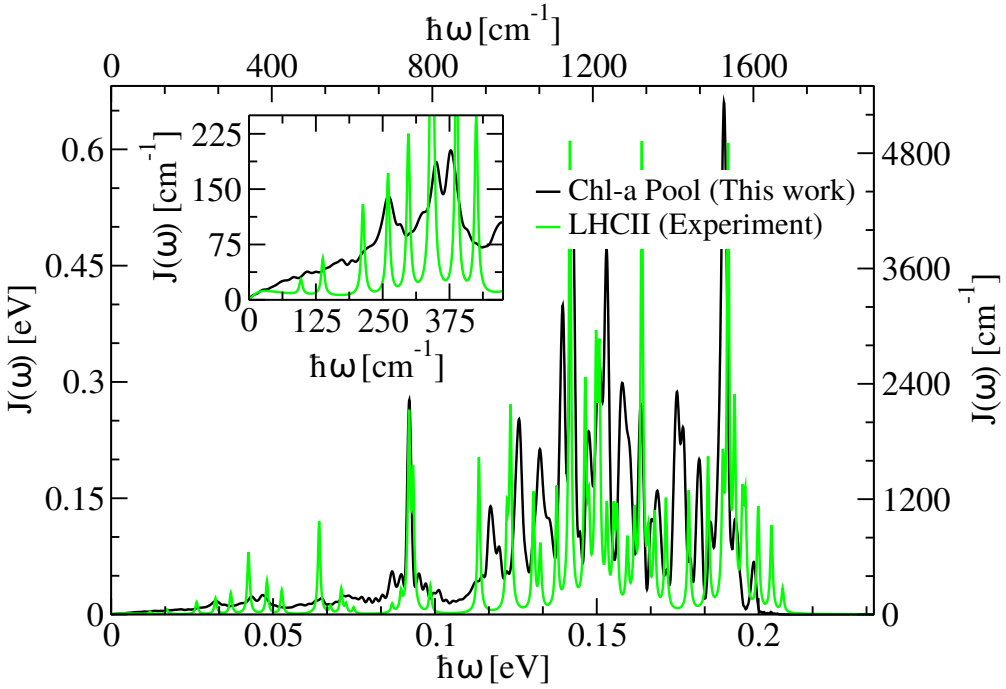

Figure 6: Comparison between the computed spectral density averaged over the Chl-a pool with the experimentally determined one based on fluorescence line narrowing (FLN) experiments of the LHCII complex[66]. The inset allows for a closer look at the low-frequency region.

experimental spectral density, the width parameter γ_k has a more or less arbitrary value controlling the broadening of the respective peaks in the high frequency region. Here, we have set its value to $\hbar\gamma_k = 7$ cm^{-1} in order to obtain peak intensities comparable to those of our computed average spectral density. In Ref. 66, this parameter was assumed to be 3 cm^{-1} whereas based on the parameters in Ref. 67, it is usually considered in theoretical modeling studies to be 10 cm^{-1} [27,68]. The fluorescence line narrowing experiments were performed for the LHCII complexes including both Chl-a and Chl-b pigments. Thus, the results could be influenced by the presence of the Chl-b molecules to some extent but because of the large structural similarity of the two pigment types one can assume that the spectral densities for both slightly different chromophores are very similar[67]. The comparison between the experimental and calculated spectral densities is given in Fig. 6. Since the crystal structure of the LHCII complex refers to a quenched state[2,49,50], we use the spectral density calculated at the low lumenal pH state for this comparison. Fig. 6 reveals an outstanding agreement

between the simulated spectral density and the respective experimental one in low and especially in the high-frequency region. The positions and intensities of most peaks display a remarkable similarity between the two variants. In the low frequency region the experimental spectral density shows more individual peaks while the theoretical counterpart shows less well separated peaks. More work on this part is needed likely from both the computational and the experimental part. For theoretical studies of the exciton transfer dynamics and spectroscopic properties, so far the experimental spectral density of the LHCII complex was utilized as input parameter[27,66–70]. Thus, to the best of our knowledge, the present study is the first attempt in which accurate spectral densities for the LHCII complex have been determined based on fully atomistic modeling. Moreover, the overall accuracy, reliability and robustness of the method applied here can be seen as a motivation for future investigations of this and similar biologically relevant LH complexes. To this end, we have employed the present results to calculate the exciton transfer rate between the pigment pair Chl-a 612 and Lut-1 (620) in order to give some insight into the experimentally observed pH-dependent regulation of the LHCII complex.

Excitation Energy Transfer Rate between Chl-a 612 and Lut-1

The LHCII complex is the major player in the NPQ mechanism in higher plants[2–5]. It has been found that the excitonic lifetime of the LHCII complex shifts from the nanosecond to the picosecond time scale when an enhanced pH gradient is built up across the thylakoid membrane. In this process, it is speculated that the pigment pair Chl-a 612 and Lut-1 (see Fig. 7) is a key player in the NPQ mechanism by releasing excess solar energy as heat[49]. NPQ is assumed to rely on the excitation energy transfer between these two pigments, while in a recent study a model involving a charge-transfer state was proposed as well[72]. In the excitonic model, the rate of the energy being transferred between the two pigments can be calculated using the Förster transfer rate $k_{m\to n}$ within the weak inter-pigment coupling limit

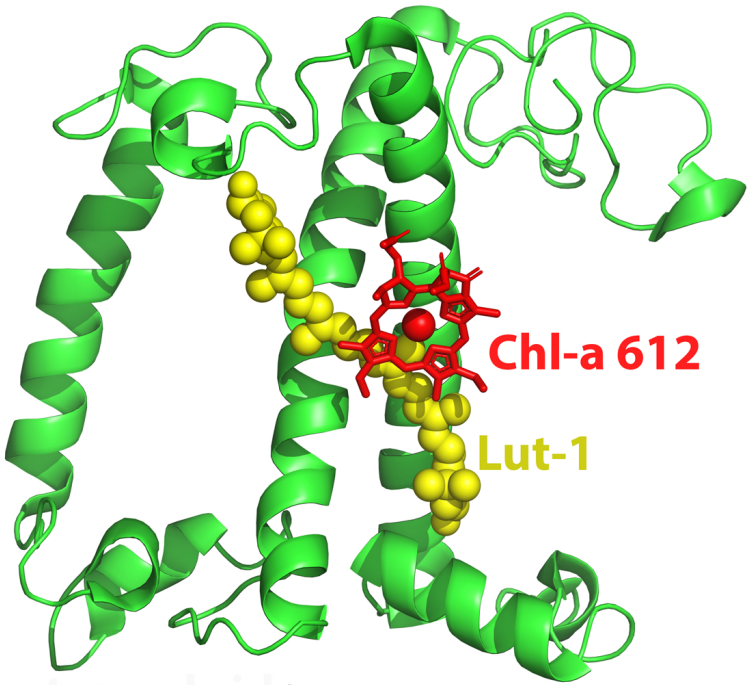

Figure 7: Structural arrangement of the pigments Chl-a 612 and Lut-1 in one monomeric subunit of the LHCII complex.

as[34,67,71,73]

$$k_{m\to n} = \frac{2}{\hbar^2}|V_{mn}|^2 \ \mathrm{Re}\int_0^\infty F_m(t)A_n(t)dt \tag{5}$$

where V_{mn} denotes the excitonic coupling between pigments m and n. The donor fluorescence F_m and the acceptor absorption A_n response functions in the time domain can be written as[34,67,71,73]

$$F_m(t) = \exp\left[-i\Big(\frac{E_m - 2\lambda_m}{\hbar}\Big)t - g_m(t)\right] \tag{6}$$

and

$$A_n(t) = \exp\left[-i\Big(\frac{E_n}{\hbar}\Big)t - g_n(t)\right] \tag{7}$$

where E_m and E_n denote the site energies of the respective donor m and the acceptor n pigments. The reorganization energy λ_m and the line-shape function $g_{m/n}$ can be directly calculated from the spectral density $J(\omega)$ as

$$\lambda_m = \int_0^\infty \frac{J_m(\omega)}{\omega}d\omega \tag{8}$$

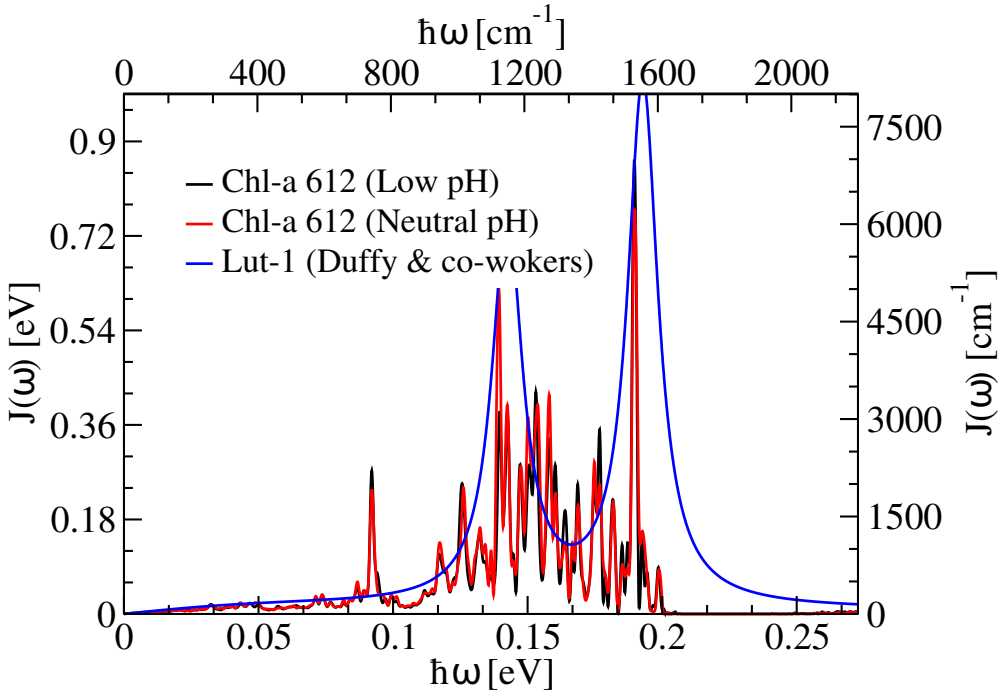

Figure 8: Spectral density of Chl-a 612 as computed in this study together with its counterpart for Lut-1 modeled from the parameters of Duffy and co-workers[71].

and

$$g_{m/n}(t) = \int_0^\infty \frac{d\omega}{\hbar\omega^2} J_{m/n}(\omega) \left[(1 - \cos(\omega t)) \coth\left(\frac{\hbar\omega}{2k_B T}\right) + i(\sin(\omega t) - \omega t) \right] . \qquad (9)$$

From the above expressions, it is clear that the site energies, excitonic coupling and the spectral densities are the main inputs to calculate the transfer rate and its inverse, i.e., the transfer time. However, the spectral density of the Lut-1 carotenoid cannot easily be determined within the DFT framework because of the failure of the DFT functionals to correctly describe the order of the exited states which include double excitation[74,75]. Although in some recent studies, DFT-based calculations were employed to explain the color tuning phenomena of carotenoids[72,76,77], we refrain here from using a DFT scheme for the calculation of carotenoid energies before having performed a proper benchmarking study. Since multiconfigurational methods are numerically too expensive to be performed along trajectories for carotenoids, here we use a model of the spectral density of Lut-1 based on experimental

findings. The functional form is the same as in Eq. 4 but now the parameters were taken from a study by Duffy and co-workers. In that work, the two-photon absorption spectrum of the carotenoid's S_1 state[78] was fitted in order to obtain the reported values[9,34,71]. Figure 8 depicts the spectral density of Lut-1 together with that of the pigment Chl-a 612 pigment from the present study. The spectral density of Lut-1 looks quite reasonable when compared to the computed Chl-a one although by far not as detailed. The main peaks are, however, at very similar frequencies even with comparable amplitudes. This finding is probably due to the fact that both molecules contain C=C bonds in their chromophoric parts. Moreover, the site energy of the dark S_1 state of Lut-1 is also taken from a fitting result of the two-photon absorption spectrum to be 14000 cm^{-1} [9,78] by Duffy and co-workers[9,34,71]. For the Chl-a 612 pigment, we have utilized the average site energies 16839 cm^{-1} and 16852 cm^{-1} at low and neutral pH values based on the TD-LC-DFTB calculations along the 1 ns-long QM/MM MD trajectory as discuss earlier.

Concerning the excitonic coupling values between the components of this special pigment pair, we have extracted the data from our previous work where the TrESP (transition charge from electrostatic potential)[75,79] method based on RASSCF transition charges[80] was applied to 500 ns-long unbiased trajectories at both pH states[9]. Since the crystal structure of the LHCII complex is quenched, the equilibrium dynamics for the neutral pH was performed starting from a selected free energy minimum as described in Ref. 9. Subsequently, based on those couplings, the spectral densities and site energies as detailed above, the excitation energy transfer rates and the corresponding transfer times between the Chl-a and Lut-1 molecules has been calculated as shown in Fig. 9. The differences in the transfer times are consistent with the pH-dependent change in the coupling since the NPQ regulation mainly depends on the conformational changes of the protein which can directly affect the coupling values but not the rest of the parameters. Differences in the transfer rates for the two pH states are clearly visible. At the same time, these changes are most likely not large enough to explain the NPQ phenomenon in total. In order to explain this phenomenon in more

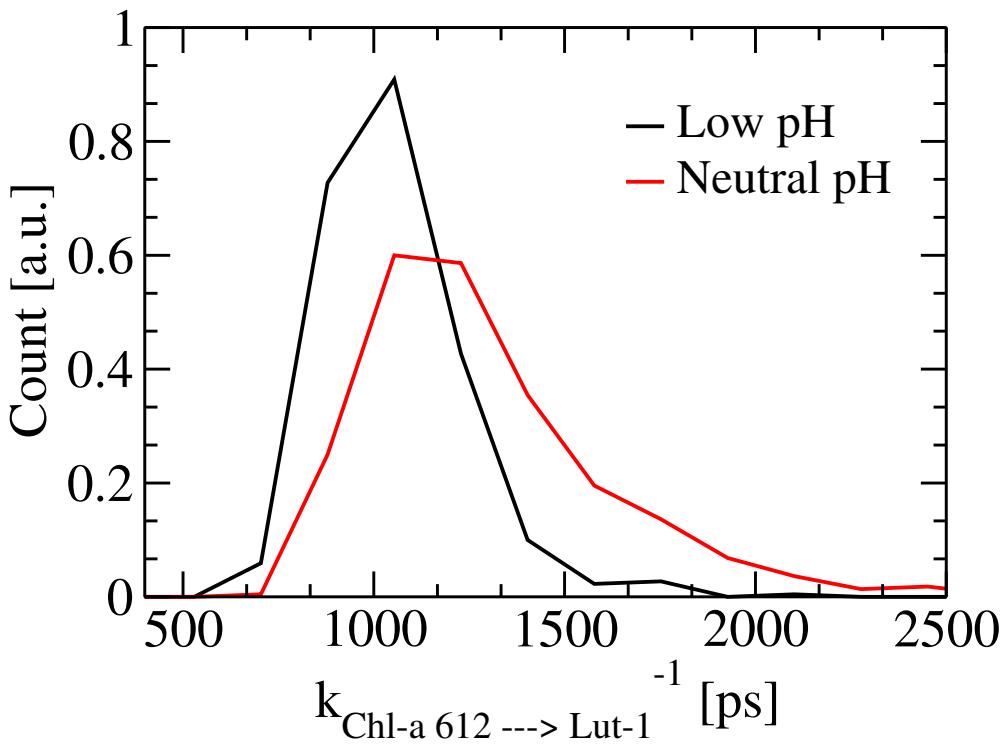

Figure 9: Excitation energy transfer rate between the pigments Chl-a 612 and Lut-1 based on the TrESP couplings extracted from Ref. 9 as well as the spectral densities and site energies for Chl-a 612 determined in this study.

detail, longer simulations might be necessary to be able to find a significant change in the coupling values between both pH states (see Fig. S5 for the coupling distribution). Moreover, a combination of EET and charge transfer mechanisms within the Chl-a/Lut-1 pair might explain the onset of the NPQ mechanism[72]. Nevertheless, the present study helps to reduce the uncertainty in one of the input parameters, i.e., the spectral density of the involved Chl-a molecule.

Conclusions

The LHCII complex balances between the light-harvesting and the photoprotective mode. In this complex, the Chl-a molecules are the major players in the energy transfer process while the carotenoids are regulators of photoprotection besides some additional light-harvesting roles. To be able to numerically determine the exciton dynamics in these processes, the

bath-induced spectral density serves as a key input within the theory of open quantum systems[20]. In order to calculate this quantity, one approach is to perform classical MD simulations followed by semi-empirical ZINDO/S-CIS or TDDFT excited state calculations. This procedure, however, is known to produce artifacts because of the poor quality ground state coordinates and dynamics. DFT-based QM/MM MD for the ground state are numerically quite expensive[25] while our recent protocol using the DFTB framework is an efficient alternative to deal with systems of the size of pigments or even larger[43]. Thus, we have performed DFTB-based QM/MM MD simulations in combination with the OPLS force field for the ground state of all Chl-a molecules in the LHCII trimer. Subsequently, TD-LC-DFTB calculations along those trajectories also in a QM/MM setting have been carried out to obtain the excitation energy fluctuations which are then utilized to determined the respective spectral densities. The results obtained with this procedure have revealed a remarkable agreement with experimental findings. Almost all major peak positions and amplitudes agree astonishingly well between theory and experiment, which clearly shows the power of the DFTB method towards the modeling of biologically LH complexes. Moreover, the present approach also has been found to be robust by reproducing the spectral densities from different starting geometries and at low and neutral lumenal pH values. Furthermore, we determined the energy ladder of the Chl-a pool which is important for studying the exciton transfer process from a sufficiently long QM/MM MD trajectory. The pigment Chl-a 610 has been found to possess the lowest site energy. At first sight, this outcome seems to be contrast with the structural orientation of the LHCII complex from which one would assume the Chl-612 to be the terminal emitter contributing lowest site energy during the energy transfer process for the Chl-a pool. At the same time, a previous theoretical study by Müh et al. suggests that Chl-a 610 can also be seen as the terminal emitter at cryogenic temperature. Moreover, at ambient temperatures the triplet Chl-a 610-611-612 is assumed to act as terminal emitter for the energy transfer process. In addition, the spectral densities and site energies have been utilized to calculate the excitation transfer rate within a pair consisting of a Chl-a 612

and a Lut-1 which is one of the key components for the allosteric regulation of the NPQ mechanism[9,49]. The trend in the rates at different pH states is consistent with our previous work[9]. The present work, however, improves the previous estimate by employing the newly determined Chl-a spectral density.

In summary, we have applied a state-of-the-art QM/MM MD technique to the LHCII complex which produces accurate results in terms of the obtained spectral density which is a key component in modeling all kind of quantum dynamical processes. So far, the experimental spectral density was mainly used to explain excitonic processes including the allosteric regulation of the LHCII complex. This is due to the numerical challenges in obtaining accurate descriptions of the spectral density, which make the numerical determination of spectral densities for large biological LH complexes still computational demanding . In this direction, the present study is the first theoretical approach where an accurate description of the spectral density is obtained for the LHCII complex. Moreover, the resulting site energies and spectral densities have also been employed to formulate a kinetic model of NPQ that involves the Chl-a 612/Lut-1 pair. This also opens the way for considering other Chl-a/carotenoid pairs in the LHCII complex.

The present study has given a hint which accuracy might be reachable in the future in modeling light-harvesting complexes of higher plants. These simulations are especially complex since one has to deal with large non-periodic complexes at least partially on a quantum mechanical level. At the same time, these complexes are rather floppy and proper sampling needs to be added as well. In the present study, for example, about 5.8 million TD-LC-DFTB calculations have been performed. In the future the assembly of several protein-pigment aggregates might shed more led on cooperative effects and how the whole machinery works together[81] as has been shown for a bacterial system recently[82].

Acknowledgments

We thank Dr. Taxiarchis Stergiannakos of Cyprus University of Technology for setting up part of the initial LHCII structures. The latter was funded through the European Regional Development Fund and the Republic of Cyprus through the Research and Innovation Foundation (Project: POST-DOC/0916/0049). The authors acknowledge support by the DFG through the joint grant EL 206/18-1 and KL-1299/18-1 as well as the DFG-Research Training groups 2247 "Quantum Mechanical Materials Modelling" and 2450 "Tailored Scale-Bridging Approaches to Computational Nanoscience".

References

(1) Blankenship, R. E. *Molecular Mechanisms of Photosynthesis*, 2nd ed.; John Wiley & Sons, 2014.

(2) Ruban, A. V.; Berera, R.; Ilioaia, C.; Van Stokkum, I. H.; Kennis, J. T.; Pascal, A. A.; Van Amerongen, H.; Robert, B.; Horton, P.; Van Grondelle, R. Identification of a Mechanism of Photoprotective Energy Dissipation in Higher Plants. *Nature* **2007**, *450*, 575.

(3) Ruban, A. V.; Johnson, M. P.; Duffy, C. D. P. The Photoprotective Molecular Switch in the Photosystem II Antenna. *Biochim. Biophys. Acta (BBA) - Bioenergetics* **2012**, *1817*, 167–181.

(4) Ruban, A. V. Light Harvesting Control in Plants. *FEBS Lett.* **2018**, *592*, 3030–3039.

(5) Tian, L.; Nawrocki, W. J.; Liu, X.; Polukhina, I.; Van Stokkum, I. H.; Croce, R. Ph Dependence, Kinetics and Light-Harvesting Regulation of Nonphotochemical Quenching in Chlamydomonas. *Proc. Nat. Acad. Sci.* **2019**, *116*, 8320–8325.

(6) Melis, A. Photosystem-II Damage and Repair Cycle in Chloroplasts: What Modulates the Rate of Photodamage in Vivo? *Trends Plant Sci.* **1999**, *4*, 130–135.

(7) Wagner, D.; Przybyla, D.; op den Camp, R.; Kim, C.; Landgraf, F.; Lee, K. P.; Würsch, M.; Laloi, C.; Nater, M.; Hideg, E., et al. The Genetic Basis of Singlet Oxygen-Induced Stress Responses of Arabidopsis Thaliana. *Science* **2004**, *306*, 1183–1185.

(8) Daskalakis, V.; Papadatos, S.; Kleinekathöfer, U. Fine Tuning of the Photosystem II Major Antenna Mobility within the Thylakoid Membrane of Higher Plants. *Biochim. Biophys. Acta - Biomembranes* **2019**, *1861*, 183059.

(9) Daskalakis, V.; Maity, S.; Hart, C. L.; Stergiannakos, T.; Duffy, C. D. P.; Kleinekathöfer, U. Structural Basis for Allosteric Regulation in the Major Antenna Trimer of Photosystem II. *J. Phys. Chem. B* **2019**, *123*, 9609–9615.

(10) Liu, Z.; Yan, H.; Wang, K.; Kuang, T.; Zhang, J.; Gui, L.; An, X.; Chang, W. Crystal Structure of Spinach Major Light-Harvesting Complex at 2.72 Å Resolution. *Nature* **2004**, *428*, 287–292.

(11) van Amerongen, H.; van Grondelle, R. Understanding the Energy Transfer Function of LHCII, the Major Light-Harvesting Complex of Green Plants. *J. Phys. Chem. B* **2001**, *105(3)*, 604–617.

(12) Kume, A.; Akitsu, T.; Nasahara, K. N. Why is Chlorophyll B Only Used in Light-Harvesting Systems? *J. Plant Res.* **2018**, *131*, 961–972.

(13) Croce, R.; van Amerongen, H. Natural Strategies for Photosynthetic Light Harvesting. *Nat. Chem. Biol.* **2014**, *10*, 492–501.

(14) Novoderezhkin, V. I.; Palacios, M. A.; van Amerongen, H.; van Grondelle, R. Excitation Dynamics in the LHCII Complex of Higher Plants: Modeling Based on the 2.72 Å Crystal Structure. *J. Phys. Chem. B* **2005**, *109*, 10493–10504.

(15) Schlau-Cohen, G. S.; Calhoun, T. R.; Ginsberg, N. S.; Read, E. L.; Ballottari, M.; Bassi, R.; van Grondelle, R.; Fleming, G. R. Pathways of Energy Flow in LHCII from Two-dimensional Electronic Spectroscopy. *J. Phys. Chem. B* **2009**, *113*, 15352–15363.

(16) Zucchelli, G.; Santabarbara, S.; Jennings, R. C. The Qy Absorption Spectrum of the Light-Harvesting Complex II as Determined by Structure-Based Analysis of Chlorophyll Macrocycle Deformations. *Biochemistry* **2012**, *51*, 2717–2736.

(17) Müh, F.; Madjet, M. E.-A.; Renger, T. Structure-based Identification of Energy Sinks in Plant Light-harvesting Complex II. *J. Phys. Chem. B* **2010**, *114*, 13517–13535.

(18) Su, X.; Ma, J.; Wei, X.; Cao, P.; Zhu, D.; Chang, W.; Liu, Z.; Zhang, X.; Li, M. Structure and Assembly Mechanism of Plant C2S2M2-type PSII-LHCII Supercomplex. *Science* **2017**, *357*, 815–820.

(19) Cao, J. et al. Quantum Biology Revisited. *Sci. Adv.* **2020**, *6*, eaaz4888.

(20) May, V.; Kühn, O. *Charge and Energy Transfer in Molecular Systems*, 3rd ed.; Wiley–VCH, 2011.

(21) Ishizaki, A.; Fleming, G. R. Theoretical Examination of Quantum Coherence in a Photosynthetic System at Physiological Temperature. *Proc. Natl. Acad. Sci. USA* **2009**, *106*, 17255–17260.

(22) Olbrich, C.; Kleinekathöfer, U. Time-Dependent Atomistic View on the Electronic Relaxation in Light-Harvesting System II. *J. Phys. Chem. B* **2010**, *114*, 12427–12437.

(23) Huo, P.; Coker, D. F. Iterative Linearized Density Matrix Propagation for Modeling Coherent Excitation Energy Transfer in Photosynthetic Light Harvesting. *J. Chem. Phys.* **2010**, *133*, 184108.

(24) Kreisbeck, C.; Kramer, T.; Rodriguez, M.; Hein, B. High-Performance Solution of

Hierarchical Equations of Motion for Studying Energy Transfer in Light-Harvesting Complexes. *J. Chem. Theory Comput.* **2011**, *7*, 2166–2174.

(25) Blau, S. M.; Bennett, D. I. G.; Kreisbeck, C.; Scholes, G. D.; Aspuru-Guzik, A. Local Protein Solvation Drives Direct Down-Conversion in Phycobiliprotein PC645 Via Incoherent Vibronic Transport. *Proc. Natl. Acad. Sci. USA* **2018**, *115*, E3342–E3350.

(26) Conti, I.; Cerullo, G.; Nenov, A.; Garavelli, M. Ultrafast Spectroscopy of Photoactive Molecular Systems from First Principles: Where We Stand Today and Where We Are Going. *J. Am. Chem. Soc.* **2020**, *142*, 16117–16139.

(27) Kreisbeck, C.; Kramer, T.; Aspuru-Guzik, A. Scalable High-Performance Algorithm for the Simulation of Exciton Dynamics. Application to the Light-Harvesting Complex II in the Presence of Resonant Vibrational Modes. *J. Chem. Theory Comput.* **2014**, *10*, 4045–4054.

(28) Olbrich, C.; Jansen, T. L. C.; Liebers, J.; Aghtar, M.; Strümpfer, J.; Schulten, K.; Knoester, J.; Kleinekathöfer, U. From Atomistic Modeling to Excitation Dynamics and Two-Dimensional Spectra of the FMO Light-Harvesting Complex. *J. Phys. Chem. B* **2011**, *115*, 8609–8621.

(29) Shim, S.; Rebentrost, P.; Valleau, S.; Aspuru Guzik, A. Atomistic Study of the Long-Lived Quantum Coherences in the Fenna-Matthew-Olson Complex. *Biophys. J.* **2012**, *102*, 649–660.

(30) Curutchet, C.; Mennucci, B. Quantum Chemical Studies of Light Harvesting. *Chem. Rev.* **2017**, *117*, 294–343.

(31) Mennucci, B.; Corni, S. Multiscale Modelling of Photoinduced Processes in Composite Systems. *Nat. Rev. Chem.* **2019**, *3*, 315–330.

(32) Segatta, F.; Cupellini, L.; Garavelli, M.; Mennucci, B. Quantum Chemical Modeling of the Photoinduced Activity of Multichromophoric Biosystems. *Chem. Rev.* **2019**,

(33) Bold, B. M.; Sokolov, M.; Maity, S.; Wanko, M.; Dohmen, P. M.; Kranz, J. J.; Kleinekathöfer, U.; Höfener, S.; Elstner, M. Benchmark and Performance of Long-Range Corrected Time-Dependent Density Functional Tight Binding (LC-TD-DFTB) on Rhodopsins and Light-Harvesting Complexes. *Phys. Chem. Chem. Phys.* **2020**, *22*, 10500–10518.

(34) Fox, K. F.; Balevičius, V.; Chmeliov, J.; Valkunas, L.; Ruban, A. V.; Duffy, C. D. The Carotenoid Pathway: What Is Important for Excitation Quenching in Plant Antenna Complexes? *Phys. Chem. Chem. Phys.* **2017**, *19*, 22957–22968.

(35) Renger, T.; Klinger, A.; Steinecker, F.; Schmidt am Busch, M.; Numata, J.; Müh, F. Normal Mode Analysis of the Spectral Density of the Fenna-Matthews-Olson Light-Harvesting Protein: How the Protein Dissipates the Excess Energy of Excitons. *J. Phys. Chem. B* **2012**, *116*, 14565–14580.

(36) Claridge, K.; Padula, D.; Troisi, A. On the Arrangement of Chromophores in Light Harvesting Complexes: Chance Versus Design. *Faraday Discuss.* **2019**, *221*, 133–149.

(37) Kim, C. W.; Choi, B.; Rhee, Y. M. Excited State Energy Fluctuations in the Fenna-Matthews-Olson Complex from Molecular Dynamics Simulations with Interpolated Chromophore Potentials. *Phys. Chem. Chem. Phys.* **2018**, *20*, 3310.

(38) Lee, M. K.; Coker, D. F. Modeling Electronic-Nuclear Interactions for Excitation Energy Transfer Processes in Light-Harvesting Complexes. *J. Phys. Chem. Lett.* **2016**, *7*, 3171–3178.

(39) Kim, C. W.; Rhee, Y. M. Constructing an Interpolated Potential Energy Surface of a Large Molecule: A Case Study with Bacteriochlorophyll a Model in the Fenna-Matthews-Olson Complex. *J. Chem. Theory Comput.* **2016**, *12*, 5235–5246.

(40) Padula, D.; Lee, M. H.; Claridge, K.; Troisi, A. Chromophore-Dependent Intramolecular Exciton-Vibrational Coupling in the FMO Complex: Quantification and Importance for Exciton Dynamics. *J. Phys. Chem. B* **2017**, *121*, 10026–10035.

(41) Rosnik, A. M.; Curutchet, C. Theoretical Characterization of the Spectral Density of the Water-Soluble Chlorophyll-Binding Protein from Combined Quantum Mechanics/Molecular Mechanics Molecular Dynamics Simulations. *J. Chem. Theory Comput.* **2015**, *11*, 5826–5837.

(42) Elstner, M.; Porezag, D.; Jungnickel, G.; Elsner, J.; Haugk, M.; Frauenheim, T.; Suhai, S.; Seifert, G. Self-consistent-charge Density-functional Tight-binding Method for Simulations of Complex Materials Properties. *Phys. Rev. B* **1998**, *58*, 7260–7268.

(43) Maity, S.; Bold, B. M.; Prajapati, J. D.; Sokolov, M.; Kubař, T.; Elstner, M.; Kleinekathöfer, U. DFTB/MM Molecular Dynamics Simulations of the FMO Light-Harvesting Complex. *J. Phys. Chem. Lett.* **2020**, *11*, 8660–8667.

(44) Kranz, J. J.; Elstner, M.; Aradi, B.; Frauenheim, T.; Lutsker, V.; Garcia, A. D.; Niehaus, T. A. Time-Dependent Extension of the Long-Range Corrected Density Functional Based Tight-Binding Method. *J. Chem. Theory Comput.* **2017**, *13*, 1737–1747.

(45) Liu, C.; Rao, Y.; Zhang, L.; Yang, C. Identification of the Roles of Individual Amino Acid Residues of the Helix E of the Major Antenna of Photosystem II (LHCII) by Alanine Scanning Mutagenesis. *J. Biochem.* **2014**, *156*, 203–210.

(46) Li, X.-P.; Gilmore, A. M.; Caffarri, S.; Bassi, R.; Golan, T.; Kramer, D.; Niyogi, K. K. Regulation of Photosynthetic Light Harvesting Involves Intrathylakoid Lumen Ph Sensing by the PsbS Protein. *J. Biol. Chem.* **2004**, *279*, 22866–22874.

(47) Bergantino, E.; Segalla, A.; Brunetta, A.; Teardo, E.; Rigoni, F.; Giacometti, G. M.; Szabo, I. Light- and pH-dependent Structural Changes in the PsbS Subunit of Photosystem II. *Proc. Natl. Acad. Sci. USA* **2003**, *100*, 15265–15270.

(48) Dolinsky, T. J.; Nielsen, J. E.; McCammon, J. A.; Baker, N. A. PDB2PQR: An Automated Pipeline for the Setup of Poisson-Boltzmann Electrostatics Calculations. *Nucleic Acids Res.* **2004**, *32*, W665–W667.

(49) Liguori, N.; Periole, X.; Marrink, S. J.; Croce, R. From Light-harvesting to Photoprotection: Structural Basis of the Dynamic Switch of the Major Antenna Complex of Plants (LHCII). *Sci. Rep.* **2015**, *5*, 15661.

(50) Pascal, A. A.; Liu, Z.; Broess, K.; van Oort, B.; van Amerongen, H.; Wang, C.; Horton, P.; Robert, B.; Chang, W.; Ruban, A. Molecular Basis of Photoprotection and Control of Photosynthetic Light-Harvesting. *Nature* **2005**, *436*, 134–137.

(51) Gaus, M.; Cui, Q.; Elstner, M. DFTB3: Extension of the Self-Consistent-Charge Density-Functional Tight-Binding Method (SCC-DFTB). *J. Chem. Theory Comput.* **2011**, *7*, 931–948.

(52) Gaus, M.; Goez, A.; Elstner, M. Parametrization and Benchmark of DFTB3 for Organic Molecules. *J. Chem. Theory Comput.* **2013**, *9*, 338–354.

(53) Kubař, T.; Welke, K.; Groenhof, G. New QM/MM Implementation of the DFTB3 Method in the Gromacs Package. *J. Comput. Chem.* **2015**, *36*, 1978–1989.

(54) Hourahine, B. et al. DFTB+, a Software Package for Efficient Approximate Density Functional Theory Based Atomistic Simulations. *J. Chem. Phys.* **2020**, *152*, 124101.

(55) Aradi, B.; Hourahine, B.; Frauenheim, T. DFTB+, a Sparse Matrix-based Implementation of the DFTB Method. *J. Phys. Chem. A* **2007**, *111*, 5678–5684.

(56) Aghtar, M.; Strümpfer, J.; Olbrich, C.; Schulten, K.; Kleinekathöfer, U. The FMO Complex in a Glycerol-Water Mixture. *J. Phys. Chem. B* **2013**, *117*, 7157–7163.

(57) Chandrasekaran, S.; Aghtar, M.; Valleau, S.; Aspuru-Guzik, A.; Kleinekathöfer, U.

Influence of Force Fields and Quantum Chemistry Approach on Spectral Densities of BChl a in Solution and in FMO Proteins. *J. Phys. Chem. B* **2015**, *119*, 9995–10004.

(58) Renger, T.; May, V.; Kühn, O. Ultrafast Excitation Energy Transfer Dynamics in Photosynthetic Pigment-Protein Complexes. *Phys. Rep.* **2001**, *343*, 137–254.

(59) Jurinovich, S.; Viani, L.; Prandi, I. G.; Renger, T.; Mennucci, B. Towards an Ab Initio Description of the Optical Spectra of Light-Harvesting Antennae: Application to the CP29 Complex of Photosystem II. *Phys. Chem. Chem. Phys.* **2015**, *17*, 14405–14416.

(60) Zhang, L.; Silva, D.-A.; Zhang, H.; Yue, A.; Yan, Y.; Huang, X. Dynamic Protein Conformations Preferentially Drive Energy Transfer Along the Active Chain of the Photosystem II Reaction Centre. *Nat. Commun.* **2014**, *5*, 4170.

(61) Ridley, J.; Zerner, M. C. An Intermediate Neglect of Differential Overlap Technique for Spectroscopy: Pyrrole and the Azines. *Theor. Chim. Acta* **1973**, *32*, 111–134.

(62) Thompson, M. A.; Zerner, M. C. A Theoretical Examination of the Electronic Structure and Spectroscopy of the Photosynthetic Reaction Center from Rhodopseudomonas Viridis. *J. Am. Chem. Soc.* **1991**, *113*, 8210–8215.

(63) Olbrich, C.; Strümpfer, J.; Schulten, K.; Kleinekathöfer, U. Theory and Simulation of the Environmental Effects on FMO Electronic Transitions. *J. Phys. Chem. Lett.* **2011**, *2*, 1771–1776.

(64) Viani, L.; Corbella, M.; Curutchet, C.; O'Reilly, E. J.; Olaya Castro, A.; Mennucci, B. Molecular Basis of the Exciton-Phonon Interactions in the PE545 Light-Harvesting Complex. *Phys. Chem. Chem. Phys.* **2014**, *16*, 16302–16311.

(65) Segatta, F.; Cupellini, L.; Jurinovich, S.; Mukamel, S.; Dapor, M.; Taioli, S.; Garavelli, M.; Mennucci, B. A Quantum Chemical Interpretation of Two-Dimensional Elec-

tronic Spectroscopy of Light-Harvesting Complexes. *J. Am. Chem. Soc.* **2017**, *139*, 7558–7567.

(66) Novoderezhkin, V.; Palacios, M. A.; van Amerongen, H.; van Grondelle, R. Energy-Transfer Dynamics in the LHCII Complex of Higher Plants: Modified Redfield Approach. *J. Phys. Chem. B* **2004**, *108*, 10363.

(67) Bennett, D. I.; Amarnath, K.; Fleming, G. R. A Structure-Based Model of Energy Transfer Reveals the Principles of Light Harvesting in Photosystem II Supercomplexes. *J. Am. Chem. Soc.* **2013**, *135*, 9164–9173.

(68) Bhattacharyya, P.; Fleming, G. R. The Role of Resonant Nuclear Modes in Vibrationally Assisted Energy Transport: The LHCII Complex. *J. Chem. Phys.* **2020**, *153*, 044119.

(69) Roden, J. J.; Bennett, D. I.; Whaley, K. B. Long-Range Energy Transport in Photosystem II. *J. Chem. Phys.* **2016**, *144*, 245101.

(70) Sláma, V.; Cupellini, L.; Mennucci, B. Exciton Properties and Optical Spectra of Light Harvesting Complex II from a Fully Atomistic Description. *Physical Chemistry Chemical Physics* **2020**, *22*, 16783–16795.

(71) Balevičius, V.; Fox, K. F.; Bricker, W. P.; Jurinovich, S.; Prandi, I. G.; Mennucci, B.; Duffy, C. D. Fine Control of Chlorophyll-Carotenoid Interactions Defines the Functionality of Light-harvesting Proteins in Plants. *Sci. Rep.* **2017**, *7*, 13956.

(72) Cupellini, L.; Calvani, D.; Jacquemin, D.; Mennucci, B. Charge Transfer from the Carotenoid Can Quench Chlorophyll Excitation in Antenna Complexes of Plants. *Nat. Commun.* **2020**, *11*, 662.

(73) Chmeliov, J.; Bricker, W. P.; Lo, C.; Jouin, E.; Valkunas, L.; Ruban, A. V.; Duffy, C.

D. P. An 'All Pigment' Model of Excitation Quenching in LHCII. *Phys. Chem. Chem. Phys.* **2015**, *17*, 15857–15867.

(74) Andreussi, O.; Knecht, S.; Marian, C. M.; Kongsted, J.; Mennucci, B. Carotenoids and Light-Harvesting: From DFT/MRCI to the Tamm-Dancoff Approximation. *J. Chem. Theory Comput.* **2015**, *11*, 655–666.

(75) Maity, S.; Gelessus, A.; Daskalakis, V.; Kleinekathöfer, U. On a Chlorophyll-Caroteinoid Coupling in LHCII. *Chem. Phys.* **2019**, *526*, 110439.

(76) Loco, D.; Buda, F.; Lugtenburg, J.; Mennucci, B. The Dynamic Origin of Color Tuning in Proteins Revealed by a Carotenoid Pigment. *J. Phys. Chem. Lett.* **2018**, *9*, 2404–2410.

(77) Bondanza, M.; Cupellini, L.; Lipparini, F.; Mennucci, B. The Multiple Roles of the Protein in the Photoactivation of Orange Carotenoid Protein. *Chem* **2019**,

(78) Walla, P. J.; Linden, P. A.; Ohta, K.; Fleming, G. R. Excited-State Kinetics of the Carotenoid S1 State in LHC II and Two-Photon Excitation Spectra of Lutein and β-carotene in Solution: Efficient Car S1$\rightarrow$ Chl Electronic Energy Transfer Via Hot S1 States? *J. Phys. Chem. A* **2002**, *106*, 1909–1916.

(79) Madjet, M. E.; Abdurahman, A.; Renger, T. Intermolecular Coulomb Couplings from Ab Initio Electrostatic Potentials: Application to Optical Transitions of Strongly Coupled Pigments in Photosynthetic Antennae and Reaction Centers. *J. Phys. Chem. B* **2006**, *110*, 17268–81.

(80) Khokhlov, D.; Belov, A. Ab Initio Model for the Chlorophyll-Lutein Exciton Coupling in the LHCII Complex. *Biophys Chem.* **2019**, *246*, 16–24.

(81) MacGregor-Chatwin, C.; Jackson, P. J.; Sener, M.; Chidgey, J. W.; Hitchcock, A.; Qian, P.; Mayneord, G. E.; Johnson, M. P.; Luthey-Schulten, Z.; Dickman, M. J.;

Scanlan, D. J.; Hunter, C. N. Membrane Organization of Photosystem I Complexes in the Most Abundant Phototroph on Earth. *Nat. Plants* **2019**, *5*, 879–889.

(82) Singharoy, A. et al. Atoms to Phenotypes: Molecular Design Principles of Cellular Energy Metabolism. *Cell* **2019**, *179*, 1098–1111.e23.

Graphical TOC Entry